Dalton Transactions

ROYAL SOCIETY OF CHEMISTRY

PAPER

View Article Online
View Journal | View Issue

Cite this: *Dalton Trans.*, 2025, **54**, 389

Evidence of boride–borylene ligand-tautomerism leading to a remote C–C-bond and concomitant boryl ligand formation†

Frerk-Ulfert Wehmeyer, [a] Yinwu Li,[b] Anne Schlossarek,[a] Zhuofeng Ke [b] and Robert Langer *[a]

Received 26th October 2024,
Accepted 28th October 2024

DOI: 10.1039/d4dt02997f

rsc.li/dalton

The formation of a rhodium pincer-type complex with a boron-based donor ligand and its reactivity are reported. The starting complex contains a formal borylene moiety, stabilised by two pyridine substituents. Quantum chemical investigations indicate the possibility of deprotonation of the central donor group of the type py_2BH in this complex. Efforts to isolate the resulting formal boride species, however, led to a boryl complex with concomitant formation of a new C–C-bond, accompanied by a loss of aromaticity. Mechanistic investigations indicate the presence of tautomerism between two deprotonated species, giving rise to a ligand-stabilised boride and a ligand-stabilised borylene motif.

Tricoordinate boron compounds usually show electrophilic and Lewis acidic properties, but in the past two decades an increasing number of nucleophilic, formally reduced boron species have been reported.[1–4] Starting with the first report of a boryl anion in 2006,[5–8] important milestones include dimetalloborylenes,[9–11] ligand-stabilised borylenes[12–16] and boroles[17] as well as the tricyanoboryl dianion, $[B(CN)_3]^{2-}$.[18,19] A common feature these compounds share is the stabilisation of a reduced, nucleophilic boron species by neutral or anionic π-accepting substituents (ligands) or metal fragments. In turn, the presence of such substituents or 'ligands' results in a rather acidic character of boron-bound hydrogen atoms in neutral borohydrides (**I**)[20] and anionic borohydrides (**II**),[21] which consequently can be deprotonated (Fig. 1a).

Nucleophilic boron compounds can serve as versatile ligands in transition[22] and main group metal complexes.[23–25] In particular, nucleophilic tri-coordinate boron compounds were demonstrated to act as anionic (**III**) or neutral (**IV**) donor ligands (Fig. 1b, L = neutral stabilising substituent, R = H, alkyl, aryl). Neutral ligand-stabilised borylenes are formally related to amines,[3] but do not show the same tendency to act as an internal base in cooperative bond activation and catalysis.[26,27] Nucleophilic boron compounds with less stabilising substituents L are usually difficult to isolate, but are still accessible by oxidative addition of ligand-stabilised boronium salts in tri-dentate pre-ligands, leading to pincer-type complexes with a central boron-based donor group (**V**).[27–31]

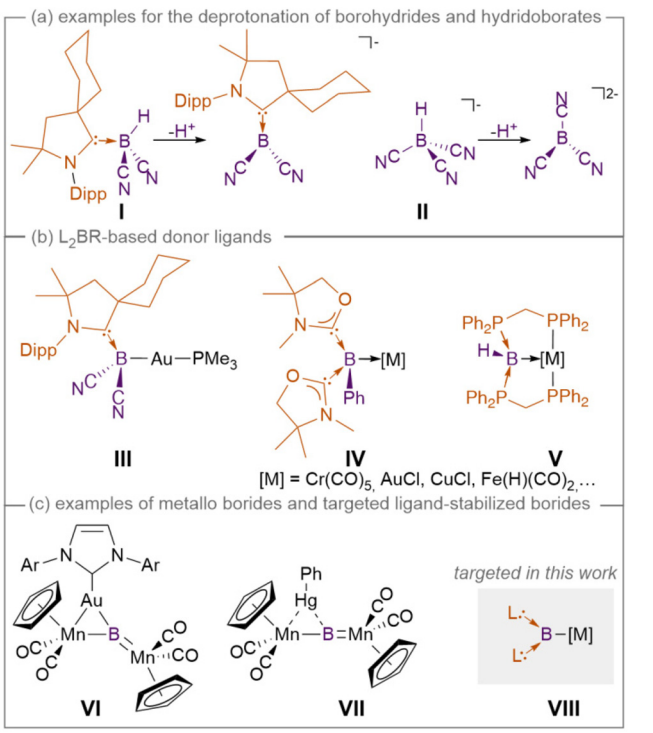

Fig. 1 Previously reported electron rich boron species.

[a]*Institute of Chemistry, Faculty of Natural Sciences II, Martin-Luther-Universität Halle-Wittenberg, Kurt-Mothes-Str. 2, D-06120 Halle (Saale), Germany. E-mail: robert.langer@chemie.uni-halle.de; Fax: +49 345 5527028; Tel: +49 345 5525620*

[b]*School of Materials Science Engineering, PCFM Lab, Sun Yat-sen University, Guangzhou 510275, China*

† Electronic supplementary information (ESI) available. CCDC 2385381–2385383. For ESI and crystallographic data in CIF or other electronic format see DOI: https://doi.org/10.1039/d4dt02997f

In analogy to the deprotonation of **I** and **II**, ligand-stabilised borylenes of the type L_2BH might be prone to deprotonation in the coordination sphere of a suitable transition metal fragment as well, resulting in a ligand-stabilised boride with a formal negative oxidation state of the central boron atom. While such boron-based ligand types are unprecedented so far, trinuclear metalla boride complexes (**VI** and **VII** in Fig. 1c) were reported by the group of Braunschweig.[32,33] Also, larger metal boride clusters are known.[34,35] In this study, we report our efforts towards the deprotonation of coordinated ligand-stabilised borylenes.

In a previous report we found for iridium complexes that complexes of type **V**, with [M] being an $Ir^{III}(Cl)(CO)(H)$-fragment, do not get straightforwardly deprotonated at the central boron-based donor group.[31] Alternative suitable ligands and metal centres, potentially capable of hosting a ligand stabilised boride, were evaluated by calculation of proton affinities of different deprotonated species using density functional theory (DFT). With respect to the calculated proton affinity (PA) of the hypothetically deprotonated iridium species with a $(R_3P)_2B$-ligand (1257 kJ mol^{-1}),[31] it was reasoned that a cationic complex with a metal centre in a low oxidation state and a π-accepting ligand in *trans*-position to the targeted boron-based ligand, as well as a more suitable set of stabilising ligands, would lead to a significantly reduced PA. We therefore targeted the corresponding rhodium(I) complexes with a square planar environment, a π-accepting carbonyl ligand in *trans*-position to the central donor group and an overall positive charge. For the established ligand system in **V**, the PA of the L_2B-species was too high (1230 kJ mol^{-1}) with respect to the undesired deprotonation at the methylene group of the $(Ph_2P)_2CH_2$ 'arm' (1171 kJ mol^{-1}) in rhodium(I) carbonyl complexes. An increased capability for π-acceptance in the analogous arsenic-based ligand with $(Ph_2As)_2CH_2$ 'arms' gave similar results and 'arm' deprotonation is more facile. We therefore turned to carbene substituents, which are capable of stabilising uncoordinated borylene species L_2BH.[12] N-heterocyclic (NHC) as well as cyclic alkyl amino carbene (CAAC) substituents decorated with PPh_2-groups resulted in lower PA values of the L_2B-anionic species of 1167 kJ mol^{-1} (NHC) and 1128 kJ mol^{-1} (CAAC). An even lower PA value of 1123 kJ mol^{-1} was calculated for stabilising pyridine groups. Considering the accessibility of pyridine-stabilised boronium precursors and the strength of the B–N-bond, the corresponding rhodium complexes were therefore targeted for synthesis.

Analogous to the previously reported procedure for the preparation of phosphine-stabilised boronium salts of the type $[(dppm)_2BH_2]^+$ (dppm = 1,1-bis(diphenylphosphinomethane))[28] we utilised pyridyldiphenylphosphane ($PyPPh_2$) instead of dppm under similar conditions. The resulting boronium salt $[(PyPPh_2)_2BH_2]Br$ (**1-Br**) was further subjected to a counter ion exchange by addition of KPF_6 to the reaction mixture, yielding **1-PF$_6$** (Fig. 2). This adjustment mitigates the issue of having multiple halide ions from different reactants in the reaction solution, which can lead to an undesired scrambling of these ions in the resulting complexes. Compared to $PyPPh_2$, the electronic environment of the phosphorus nuclei in $[(PyPPh_2)_2BH_2]^+$ (**1**) exhibits only a minor change indicated by similar chemical shifts in the $^{31}P\{^1H\}$ NMR spectrum (−4.9 *vs.* −7.1 ppm). A broadened resonance at −1.9 ppm in the $^{11}B\{^1H\}$ NMR spectrum is consistent with the boronium salt stabilised by two pyridine groups (2.1 ppm).[36] The ^1H NMR spectrum of **1** displays all resonances associated with pyridyl and phenyl rings as well as broadened two proton resonance for the boron-bound hydrogen atoms. The structural identity of **1-X** was also confirmed by single-crystal X-ray diffraction.[37]

The reaction of **1** with $[RhCl(CO)_2]_2$ yields a mixture of products. With 1,4-diazabicyclo[2.2.2]octane (DABCO) as an auxiliary base, the complex $[(HB\{PPh_2Py\}_2)Rh(CO)_2]PF_6$ (**2**) is obtained as the predominant product, as indicated by the $^{31}P\{^1H\}$ NMR spectroscopy. Specifically, in addition to the typical septet associated with the PF_6^- counterion, only a doublet at 49.7 ppm is observed. This indicates that both phosphorus atoms are chemically equivalent and are coupling to the rhodium with a coupling constant of $^1J_{PRh}$ = 163.8 Hz, which is typical for rhodium(I) complexes.[38] A broad signal at 17.0 ppm is observed in the $^{11}B\{^1H\}$ NMR spectrum. The ^1H NMR spectrum shows resonances of both, phenyl and pyridyl protons. The shift of the boron-bound proton at 5.11 ppm is broadened with a peak integration corresponding to one proton, indicating that the boronium species was deprotonated during the reaction, which is consistent with previously published syntheses.[27,28,30,31] Single-crystal X-ray diffraction reveals a trigonal bipyramidal coordination geometry of the rhodium centre in **2** with a tri-dentate PBP-type ligand and two carbonyl ligands (τ_5 = 0.85).[39] The central boron atom exhibits a tetrahedral environment with a sum of angles between the substituents close to 300°.

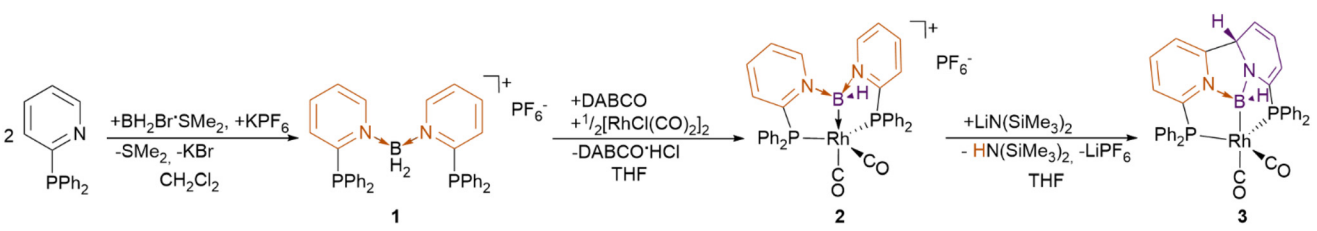

Fig. 2 Oxidative addition of the pyridine-stabilised boronium salt **1**, resulting in the formation of complex **2**, which can be deprotonated with $LiN(SiMe_3)_2$.

Utilisation of methyllithium as a base for the deprotonation of **2** results in an unselective reaction and the formation of numerous products is indicated by the $^{31}P\{^{1}H\}$ NMR spectrum of the reaction mixture. *In situ* high-resolution mass spectrometry (HR-MS) suggests that methylation takes place, rather than deprotonation with MeLi. In accordance with reactions known from the literature, this could have taken place in the α-position of the pyridines.[40–42]

With $LiN(SiMe_3)_2$ or KO*t*Bu as the base, a new complex (**3**) selectively formed and was isolated *via* crystallisation. Single-crystal X-ray diffraction reveals distinct differences with respect to complex **2**: a new C–C-bond is formed between the two N-heterocycles at positions α and α′ with a length of 1.533 Å, which is a typical distance for a C–C single bond. One of the rings, along with its adjacent atoms, remains a planar pyridine moiety with a new C–C-instead of a C–H-bond, indicating a deprotonation at this position during the reaction. The C–C-bond distances of 1.379–1.393 Å are consistent with those observed for the pyridyl groups in **2** (1.363–1.391 Å). In the second ring, the planar structure of the former pyridine moiety is disturbed. Only four carbon atoms are located in a slightly distorted plane, resulting in a butadiene-like system. This is supported by the ene-bond distances (1.333–1.350 Å), which are showing the only π-conjugation in this heterocycle. Compared to the pyridine system in **2**, the other C–C-bonds in the cycle are elongated (1.449–1.501 Å); this also applies for the C–N-bonds (1.388–1.485 Å). The carbon at the α-position is tetrahedrally bound as a result of the newly formed C–C-bond. The neighbouring nitrogen atom is pyramidalised, indicating the presence of a non-coordinating lone pair. The corresponding B–N-bond is shortened (1.543 Å) compared to the donating pyridyl groups in **2** (1.613–1.628 Å) as well as the bond formed by the planar pyridyl group in **3** (1.609 Å). As the ligand in **3** is formed by deprotonation and is formally anionic, the non-planar, de-aromatised structure of the second N-heterocycle indicates the formation of an anionic amido substituent. These findings are in line with an overall anionic ligand- or base-stabilised boryl ligand in **3** that has been formed upon deprotonation. A spectrum of higher order is observed by $^{31}P\{^{1}H\}$ NMR spectroscopy, implying that the phosphorus atoms are no longer chemically equivalent. In the ^{1}H NMR spectrum, the peak integrals for the aromatic resonances of the pyridyl group are consistent with three protons in the remaining pyridine ring. The four resonances between 4.69 and 6.14 ppm, each with a peak integral corresponding to one proton, point to the de-aromatised N-heterocycle, the former pyridine group in **2**. Notably, the proton in α-position to the nitrogen atom gives rise to a chemical shift of 5.22 ppm, which is an unusually low field shift for an aliphatic proton. This can be attributed to the delocalised π-systems of the adjacent carbon and nitrogen atoms. A resonance for the boron-bound hydrogen atom is observed at 4.51 ppm in the ^{1}H NMR spectrum and the $^{1}B\{^{1}H\}$ NMR spectrum of **3** exhibits a resonance at 13.3 ppm.

The C–C-bond formation between two coordinated pyridyl groups has already been reported in the coordination sphere of rhenium.[43,44] In these cases, the deprotonation and bond formation lead to unstable products, which are only isolatable after oxidative re-aromatisation or protonation in the case of steric hindrance. The observation of this reaction in the coordination sphere of the main group element boron underlines the ability of reduced boron species to mimic the reactivity of transition metals, such as the recently reported activation of N_2.[45]

Complex **3** turns out to be surprisingly stable and attempts to abstract dihydrogen using common hydrogen acceptors like FLPs (frustrated Lewis pair) and acetylenes showed no reaction. This is particularly notable, as restoring the aromaticity of the heterocycle is typically a strong driving force in similar systems.[43,44] As the elimination of dihydrogen is thermodynamically feasible, according to our DFT calculations, the observed stability appears to originate from a kinetic stabilisation.

Comparing **2** and **3**, the similarity in their structures is striking. Single-crystal X-ray diffraction reveals that the distortion in the ligand backbone, caused by C–C-bond formation, has only a minor effect on the overall geometric arrangement (Fig. 3). In both cases, the boron species exhibits a tetrahedral arrangement. Remarkably, the metal centres show only slight differences in their geometric arrangement, as the positions of

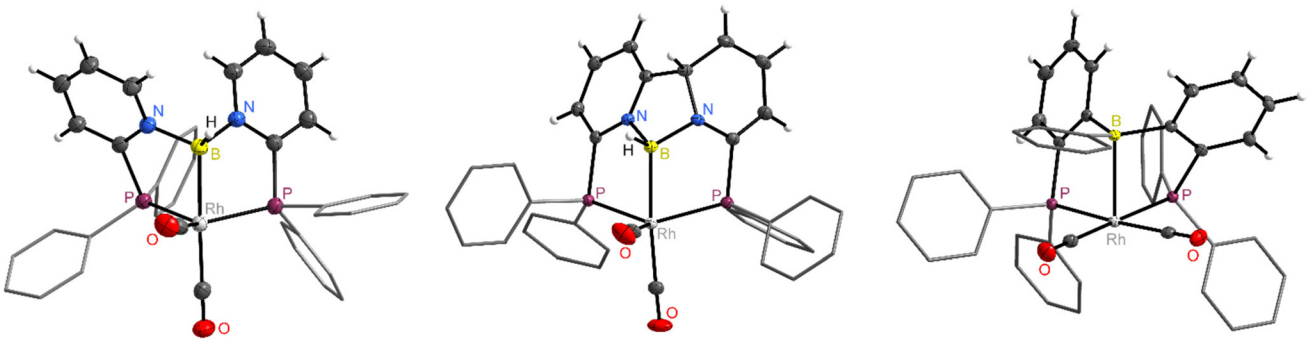

Fig. 3 Molecular structure of **2** (left) and **3** (middle) and a previous work by Conifer **4** (right) measured by X-ray single crystal diffraction in the solid state. Phenyl rings are reduced to their frame, and solvents from crystallisation and counter ions are omitted for clarity.

all ligands remain largely unchanged. Both complexes display a trigonal bipyramidal arrangement, with P–Rh–P angles of 114.06° in **2** and 124.12° in **3**, which are close to the ideal trigonal angle of 120°. The geometry index[39] τ of 0.85 for **2** and 0.80 for **3** supports this observation. The geometric arrangement at the boron and rhodium centres indicates that neither **2** nor **3** exhibits characteristics of a Z-type complex, where rhodium would donate electron density to the boron.[46] To illustrate this contrast, a similar complex $[Rh(CO)_2(BPP)]SbF_6$ (BPP = $PhB(C_6H_4PPh_2)_2$) (**4**) with a related Z-type boron-based ligand, reported by Conifer,[47] is used for comparison to identify potential differences between the ligand types (Table 1). Like complexes **2** and **3**, complex **4** is a PBP-type rhodium(I) pincer complex with two additional carbonyl ligands, however with the boron covalently bonded to three carbon atoms, making it a borane species. The geometrical arrangement of the borane-based ligand is trigonal planar, with rhodium vertically donating electron density to a vacant p-orbital at the boron atom. This results in a square pyramidal arrangement at the central rhodium atom with the borane at the apex (τ = 0.03), consistent with an occupied d_{z^2} orbital of the rhodium that forms the dative bond to the borane. Comparison of these $(PBP)Rh(CO)_2$ complexes (**2–4**) clearly shows that with L- and X-type ligands, a trigonal bipyramidal arrangement is more favourable, whereas the Z-type ligand gives rise to square pyramidal coordination geometry. The L-type ligand in **2** gives rise to the shortest Rh–B-bond (2.198(5) Å), which is in the range of typical borylene metal bonds (2.115–2.342 Å),[23,27–31,48,49] followed by a slightly longer Rh–B-bond in **3** (2.229(2) Å), whereas the Rh–B-bond to the Z-type ligand in **4** is significantly longer at 2.449(3) Å.[50–56] The different nature of the boron-based ligands **2–4** is also reflected in a different degree of pyramidalisation of the central boron atom, which can be measured by the sum of the angles between the organic substituents. In line with a rather weak interaction and a long bond distance, the Z-type ligand in **4** exhibits an almost trigonal planar environment ($\sum\alpha_B$ = 351.7°), whereas the L- and X-type ligands in **2** and **3** contain strongly pyramidalised boron atoms with $\sum\alpha_B$ below 300°.

$^{11}B\{^1H\}$ NMR spectroscopy reveals a trend for the chemical shifts for the coordinated boron-based ligands decreasing from the L-type (17.0 ppm) to the X-type (13.3 ppm) and the Z-type (−0.5 ppm). The value of the $^1J_{RhP}$ coupling constant is sensitive to the s-orbital's contribution to the Rh–P-bond and provides information about formal oxidation states.[57–61] The value of 163.8 Hz in **2** is consistent with a rhodium(I) complex, but the coupling constant in **4** is between the typical values for rhodium(I) and rhodium(III).

Further insights into the bond situation in **2–4** were obtained by quantum chemical investigations, using density functional theory on the B97D3/def2-TZVPP level of theory. Partial charges obtained by natural population analysis (NPA) were calculated to be similar for the neutral ligand in **2** (q_B = 0.43) and the anionic ligand in **3** (q_B = 0.46), but a more positive value is obtained for the Z-type ligand in **4** (q_B = 0.86). The bonding situation was further analysed by the quantum theory of atoms in molecules (QTAIM). Fig. 4 shows the Laplacian distribution of the electron density of the Rh–B–N/C-plane in **2–4**. It becomes evident that both the L- and the X-type ligands show a charge accumulation located before the bond critical point of the Rh–B-bond, clearly indicating the electron-donating nature of the boron-based ligands in both complexes. In contrast, no charge accumulation is observed at the boron atom for the Z-type ligand in **4**. In addition, a curved bond path was found, suggesting a comparably weak interaction between rhodium and boron in **4**. Overall, the trends observed for rhodium complexes **2–4** reproduce well the findings in previously investigated palladium complexes and clearly show differences between the ligand types according to the covalent bond classification.[28] The similarity of the charge distribution in **2** and **3** is also underlined by cyclic voltammetry measurements, where the oxidation potentials *vs.* Fc/Fc^+ of **2** (+0.16 V) and **3** (+0.21 V) are quite alike.

Despite the low PA-value of the targeted ligand with pyridine substituents no deprotonation of the Py_2BH-ligand could be observed. To understand the reasons for the observed selectivity, we calculated potential pathways for the deprotonation of **2** by the $N(SiMe_3)_2$-anion, using density functional theory (DFT) at the B97D3/def2-TZVP level of theory (Fig. 5). Ion pair formation from **2** and $[N(SiMe_3)_2]^-$ in dichloro-

Table 1 Comparison of selected properties of L-, X- and Z-type boron-based ligands rhodium complexes of the type $[(PBP)Rh(CO)_2]^n$

Complex	**2**	**3**	**4**
Ligand type	L	X	Z
d_{Rh-B}/Å	2.198(5)	2.229(2)	2.449(3)
d_{Rh-P}/Å	2.285(1), 2.267(1)	2.305(1), 2.296(1)	2.312(1), 2.360(1)
$\sum\alpha_B$/°	298.6	296.5	351.7
τ_5	0.85	0.80	0.03
δ_B/ppm	17.0	13.3	−0.5
δ_P/ppm	49.9	59.8	35.5
$^1J_{RhP}$/Hz	163.8	—	119.3
$\tilde{\nu}$ (CO)/cm^{-1}	2018, 1956	1986, 1934	2123, 2096
q_B (NBO)	0.43	0.46	0.89

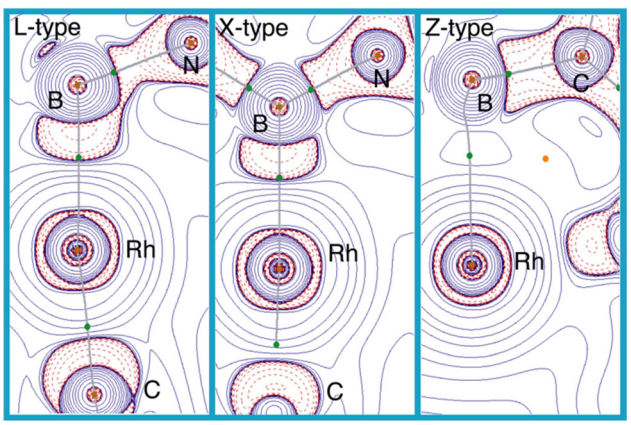

Fig. 4 Laplacian distribution of the electron density in **2** (L-type), **3** (X-type) and **4** (L-type).

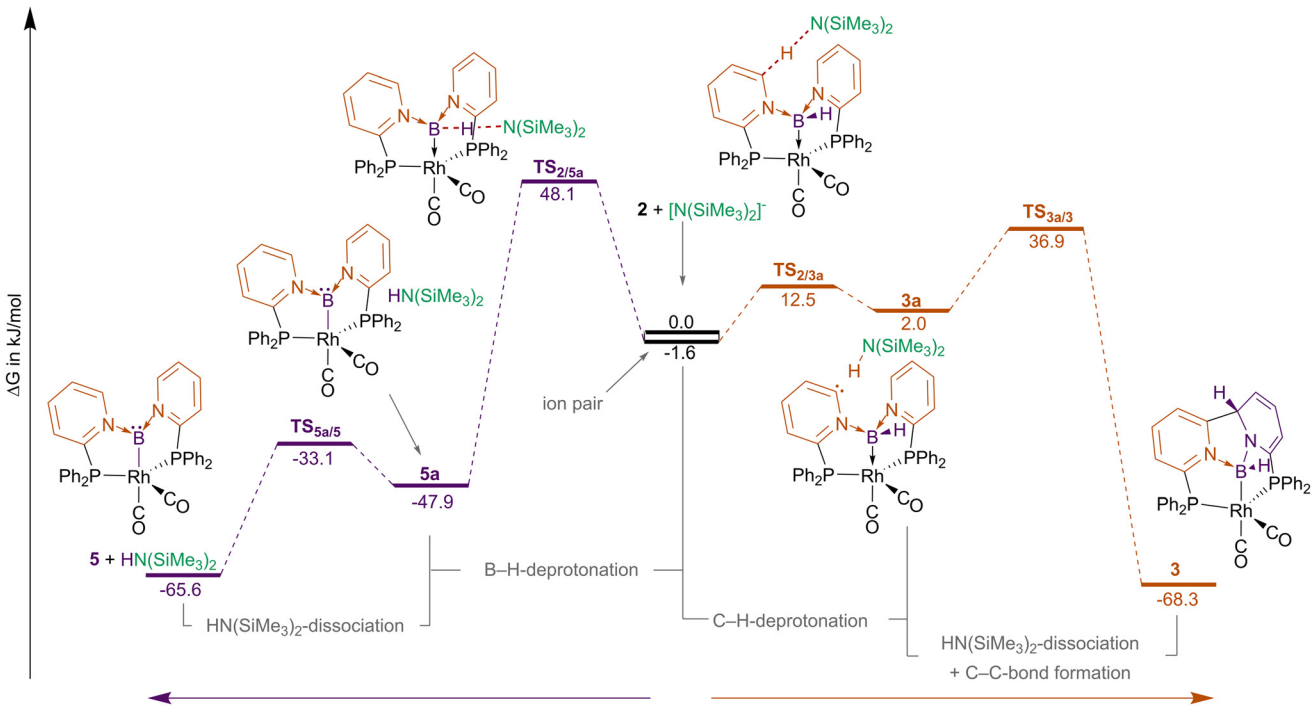

Fig. 5 Calculated possible pathways for the deprotonation of **2**. Left: The deprotonation at the boron leads to a boride species **5** *via* $HN(SiMe_3)_2$-stabilised intermediate **5a**. Right: The deprotonation at position 6 at the pyridine ring results in $HN(SiMe_3)_2$-stabilised intermediate **3a**, followed by dissociation and C–C-bond formation leading to **3** (ΔG values are given in kJ mol^{-1}).

methane (DCM) was calculated to be only slightly exergonic by −1.6 kJ mol^{-1}. Starting from this ion pair, two potential pathways for deprotonation were explored, one leading to a deprotonated boron species (**5a**) and the other to a deprotonated pyridine species (**3a**) as well as $HN(SiMe_3)_2$ in close proximity, respectively. Our calculations show that deprotonation of the Py_2BH-group in **2** and formation of **5a** is thermodynamically preferred with a relative Gibbs free energy of ΔG_{rel} = −47.9 kJ mol^{-1}, whereas the deprotonation in 6-position of one of the pyridine rings in **2** is even slightly endergonic (ΔG_{rel} = −2.0 kJ mol^{-1}). However, although the barrier for BH-deprotonation in **2** *via* $\mathbf{TS_{2/5a}}$ is not very high ($\Delta G^{\ddagger}_{rel}$ = 48.1 kJ mol^{-1}), the barrier for pyridine ring deprotonation *via* $\mathbf{TS_{2/3a}}$ is significantly lower ($\Delta G^{\ddagger}_{rel}$ = 12.5 kJ mol^{-1}), showing a kinetic preference for pyridine ring deprotonation. Overall, the calculated differences in Gibbs energy and reaction barriers for the proton transfer *via* $HN(SiMe_3)_2$ are comparably low, suggesting the possibility for a tautomeric equilibrium between a ligand-stabilised boride ligand in **5a** and a pyridyl-/pyridinyl-stabilised boryl ligand in **3a**.

The $HN(SiMe_3)_2$-dissociation from **5a** proceeds with a low barrier of $\Delta G^{\ddagger}_{rel}$ = 14.8 kJ mol^{-1} *via* $\mathbf{TS_{5a/5}}$ with respect to **5a**, leading to **5**. The dissociation of $HN(SiMe_3)_2$ from **3a** *via* $\mathbf{TS_{3a/3}}$ exhibits a higher barrier of $\Delta G^{\ddagger}_{rel}$ = 34.9 kJ mol^{-1} and initiates the formation of the C–C-bond between the pyridine rings in **3**. The calculated difference in Gibbs energy of the two deprotonation products **3** and **5** is very small with $\Delta\Delta G$ = 2.7 kJ mol^{-1}, suggesting that the formation of pyridine-stabilised boride ligands should in principle be facile. However, in the current reported case the desired B–H deprotonation is kinetically not favourable.

To obtain further insights into the deprotonation of **2**, we investigated the formation of **3** as a function of temperature using *in situ* UV/vis spectroscopy. Solutions of **2** and LiHMDS were mixed at −40 °C and allowed to warm up.[37] From −10 °C onwards, the spectra began to change from the initial state. By plotting the deviation from the starting spectrum, these plots are proportional to the difference between the spectra of **2** and **3**. This indicates that no intermediate species with significant absorbance in the measured range is present, which would otherwise affect this correlation. In comparison with other tautomeric equilibria, such as the keto–enol-tautomerism, the reaction barriers between **3a** and **5a** are small and the initial deprotonation product **5a** is even thermodynamically more stable than **3a**. Although in most cases the enol form is thermodynamically less stable with respect to the keto form, it is important for the reactivity of carbonyl compounds in general. For this reason, a boride-based reactivity might be possible for the ligand system reported herein as well.

Conclusions

In conclusion, a rationale for the stabilisation of donor-stabilised boride (L_2B^-) as a ligand was presented and pyridine was identified as the preferential stabilising donor. The synthesised electron-rich borylene complex **2** with two stabilising

pyridine moieties can form two tautomeric products, **3a** and **5a**, upon deprotonation. Quantum chemical investigations revealed that the irreversible formation of a remote C–C-bond between the two pyridine substituents in **3** is kinetically favoured. The possibility for the presence of a tautomerism involving boron species has never been reported and the reactivity observed for these species is unprecedented. Furthermore, the comparison of different properties of the obtained ligand types in the context of the covalent bond classification revealed distinct differences between σ-accepting (Z-type) and σ-donating (L- and X-type) boron-based ligands. Our study prompts us to make further ligand adjustments in order to hamper pyridine deprotonation and drive the reaction toward boride formation.

Author contributions

F. W., Y. L. and A. S. carried out the synthetic work, and performed and interpreted the analytical characterizations. R. L. carried out and analysed the computational studies. F. W. carried out the X-ray diffraction studies. R. L. supervised the project. Z. K. co-supervised the project. F. W. wrote the initial draft of the manuscript. All authors contributed to the writing of the manuscript and validated it prior to submission.

Data availability

The data supporting this article have been included as part of the ESI.† Crystallographic data for **1–3** have been deposited at the Cambridge Crystallographic Data Centre (CCDC) under CCDC 2385381–2385383† and can be obtained from **https://www.ccdc.cam.ac.uk/**.

Conflicts of interest

There are no conflicts to declare.

Acknowledgements

R. L. is grateful to the Deutsche Forschungsgemeinschaft (DFG) for supporting this research (LA 2830/6-2) and for funding within the Heisenberg program (LA 2830/9-1).

Notes and references

1 L. Weber, *Eur. J. Inorg. Chem.*, 2012, 5595–5609.
2 J. Cid, H. Gulyás, J. J. Carbó and E. Fernández, *Chem. Soc. Rev.*, 2012, **41**, 3558.
3 M. Soleilhavoup and G. Bertrand, *Angew. Chem., Int. Ed.*, 2017, **56**, 10282–10292.
4 M. Arrowsmith, H. Braunschweig and T. E. Stennett, *Angew. Chem., Int. Ed.*, 2017, **56**, 96–115.
5 Y. Segawa, M. Yamashita and K. Nozaki, *Science*, 2006, **314**, 113–115.
6 T. B. Marder, *Science*, 2006, **314**, 69–70.
7 H. Braunschweig, *Angew. Chem., Int. Ed.*, 2007, **46**, 1946–1948.
8 T. Ohsato, Y. Okuno, S. Ishida, T. Iwamoto, K. Lee, Z. Lin, M. Yamashita and K. Nozaki, *Angew. Chem., Int. Ed.*, 2016, **55**, 11426–11430.
9 D. L. Coombs, S. Aldridge and C. Jones, *J. Chem. Soc., Dalton Trans.*, 2002, 3851.
10 H. Braunschweig, M. Burzler, R. D. Dewhurst and K. Radacki, *Angew. Chem., Int. Ed.*, 2008, **47**, 5650–5653.
11 D. Vidovic and S. Aldridge, *Angew. Chem., Int. Ed.*, 2009, **48**, 3669–3672.
12 R. Kinjo, B. Donnadieu, M. A. Celik, G. Frenking and G. Bertrand, *Science*, 2011, **333**, 610–613.
13 F. Dahcheh, D. Martin, D. W. Stephan and G. Bertrand, *Angew. Chem., Int. Ed.*, 2014, **53**, 13159–13163.
14 L. Kong, Y. Li, R. Ganguly, D. Vidovic and R. Kinjo, *Angew. Chem., Int. Ed.*, 2014, **53**, 9280–9283.
15 M. Soleilhavoup and G. Bertrand, *Acc. Chem. Res.*, 2015, **48**, 256–266.
16 H. Braunschweig, R. D. Dewhurst, F. Hupp, M. Nutz, K. Radacki, C. W. Tate, A. Vargas and Q. Ye, *Nature*, 2015, **522**, 327–330.
17 H. Braunschweig, C. Chiu, K. Radacki and T. Kupfer, *Angew. Chem., Int. Ed.*, 2010, **49**, 2041–2044.
18 J. Landmann, J. A. P. Sprenger, R. Bertermann, N. Ignat'ev, V. Bernhardt-Pitchougina, E. Bernhardt, H. Willner and M. Finze, *Chem. Commun.*, 2015, **51**, 4989–4992.
19 E. Bernhardt, V. Bernhardt-Pitchougina, H. Willner and N. Ignatiev, *Angew. Chem., Int. Ed.*, 2011, **50**, 12085–12088.
20 D. A. Ruiz, G. Ung, M. Melaimi and G. Bertrand, *Angew. Chem., Int. Ed.*, 2013, **52**, 7590–7592.
21 J. Landmann, F. Keppner, D. B. Hofmann, J. A. P. Sprenger, M. Häring, S. H. Zottnick, K. Müller-Buschbaum, N. V. Ignat'ev and M. Finze, *Angew. Chem., Int. Ed.*, 2017, **56**, 2795–2799.
22 H. Braunschweig, R. D. Dewhurst and V. H. Gessner, *Chem. Soc. Rev.*, 2013, **42**, 3197.
23 H. Braunschweig, R. D. Dewhurst, L. Pentecost, K. Radacki, A. Vargas and Q. Ye, *Angew. Chem., Int. Ed.*, 2016, **55**, 436–440.
24 A.-F. Pécharman, A. L. Colebatch, M. S. Hill, C. L. McMullin, M. F. Mahon and C. Weetman, *Nat. Commun.*, 2017, **8**, 15022.
25 M. Häring, C. Kerpen, T. Ribbeck, P. T. Hennig, R. Bertermann, N. V. Ignat'ev and M. Finze, *Angew. Chem., Int. Ed.*, 2022, **61**, e202202882.
26 L. Vondung, N. Frank, M. Fritz, L. Alig and R. Langer, *Angew. Chem., Int. Ed.*, 2016, **55**, 14450–14454.
27 A. Bäcker, Y. Li, M. Fritz, M. Grätz, Z. Ke and R. Langer, *ACS Catal.*, 2019, **9**, 7300–7309.
28 M. Grätz, A. Bäcker, L. Vondung, L. Maser, A. Reincke and R. Langer, *Chem. Commun.*, 2017, **53**, 7230–7233.
29 L. Maser, C. Schneider, L. Vondung, L. Alig and R. Langer, *J. Am. Chem. Soc.*, 2019, **141**, 7596–7604.

30 F.-U. Wehmeyer and R. Langer, *Chem. Commun.*, 2023, **59**, 6004–6007.
31 L. Maser, C. Schneider, L. Alig and R. Langer, *Inorganics*, 2019, **7**, 61.
32 H. Braunschweig, P. Brenner, R. D. Dewhurst, M. Kaupp, R. Müller and S. Östreicher, *Angew. Chem., Int. Ed.*, 2009, **48**, 9735–9738.
33 R. Bertermann, H. Braunschweig, W. C. Ewing, T. Kramer, A. K. Phukan, A. Vargas and C. Werner, *Chem. Commun.*, 2014, **50**, 5729.
34 F. E. Hong, T. J. Coffy, D. A. McCarthy and S. G. Shore, *Inorg. Chem.*, 1989, **28**, 3284–3285.
35 C. E. Housecroft, *Coord. Chem. Rev.*, 1995, **143**, 297–330.
36 O. P. Shitov, V. A. Tartakovskii and S. L. Ioffe, *Chem. Heterocycl. Compd.*, 2015, **50**, 1647–1657.
37 ESI.†
38 T. H. Brown and P. J. Green, *J. Am. Chem. Soc.*, 1970, **92**, 2359–2362.
39 A. W. Addison, T. N. Rao, J. Reedijk, J. Van Rijn and G. C. Verschoor, *J. Chem. Soc., Dalton Trans.*, 1984, 1349–1356.
40 K. Schmalzl and L. Summers, *Aust. J. Chem.*, 1977, **30**, 657.
41 K. Ogawa, Y. Takeuchi, H. Suzuki and Y. Nomura, *J. Am. Chem. Soc.*, 1984, **106**, 831–841.
42 F. Louërat, Y. Fort and V. Mamane, *Tetrahedron Lett.*, 2009, **50**, 5716–5718.
43 M. Espinal Viguri, M. A. Huertos, J. Pérez, L. Riera and I. Ara, *J. Am. Chem. Soc.*, 2012, **134**, 20326–20329.
44 M. E. Viguri, J. Pérez and L. Riera, *Chem. – Eur. J.*, 2014, **20**, 5732–5740.
45 M.-A. Légaré, G. Bélanger-Chabot, R. D. Dewhurst, E. Welz, I. Krummenacher, B. Engels and H. Braunschweig, *Science*, 2018, **359**, 896–900.
46 A. Amgoune and D. Bourissou, *Chem. Commun.*, 2011, **47**, 859–871.
47 C. M. Conifer, D. J. Law, G. J. Sunley, A. J. P. White and G. J. P. Britovsek, *Organometallics*, 2011, **30**, 4060–4066.
48 L. Kong, W. Lu, L. Yongxin, R. Ganguly and R. Kinjo, *Inorg. Chem.*, 2017, **56**, 5586–5593.
49 M. Zweigart, K. Eichele, H. Schubert, C. P. Sindlinger and L. Wesemann, *J. Am. Chem. Soc.*, 2023, **145**, 12452–12458.
50 A. F. Hill, G. R. Owen, A. J. P. White and D. J. Williams, *Angew. Chem., Int. Ed.*, 1999, **38**, 2759–2761.
51 J. S. Figueroa, J. G. Melnick and G. Parkin, *Inorg. Chem.*, 2006, **45**, 7056–7058.
52 R. J. Blagg, J. P. H. Charmant, N. G. Connelly, M. F. Haddow and A. G. Orpen, *Chem. Commun.*, 2006, 2350–2352.
53 M. Sircoglou, S. Bontemps, M. Mercy, N. Saffon, M. Takahashi, G. Bouhadir, L. Maron and D. Bourissou, *Angew. Chem., Int. Ed.*, 2007, **46**, 8583–8586.
54 G. R. Owen, P. H. Gould, A. Hamilton and N. Tsoureas, *Dalton Trans.*, 2010, **39**, 49–52.
55 A. Zech, M. F. Haddow, H. Othman and G. R. Owen, *Organometallics*, 2012, **31**, 6753–6760.
56 N. Hara, K. Yamamoto, Y. Tanaka, T. Saito, S. Sakaki and Y. Nakao, *Bull. Chem. Soc. Jpn.*, 2021, **94**, 1859–1868.
57 N. Muller and D. E. Pritchard, *J. Chem. Phys.*, 1959, **31**, 768–771.
58 J. N. Shoolery, *J. Chem. Phys.*, 1959, **31**, 1427–1428.
59 D. Cremer and J. Gräfenstein, *Phys. Chem. Chem. Phys.*, 2007, **9**, 2791–2816.
60 L. C. Ducati, A. Marchenko and J. Autschbach, *Inorg. Chem.*, 2016, **55**, 12011–12023.
61 A. Obeng and J. Autschbach, *J. Chem. Theory Comput.*, 2024, **20**, 4965–4976.